Searches for dark matter at the LHC: A multivariate analysis in the mono-Z channel

Alexandre Alves and Kuver Sinha

Searches for Dark Matter at the LHC: A Multivariate Analysis in the Mono-Z Channel

Alexandre Alves[1] and Kuver Sinha[2]

[1]*Departamento de Ciências Exatas e da Terra,*
Universidade Federal de São Paulo, 09972-270, Diadema-SP, Brasil
[2]*Department of Physics, Syracuse University, Syracuse, NY 13244, USA*
(Dated: October 19, 2015)

We study dark matter (DM) production in the mono-Z channel at the 13 TeV LHC both in an effective field theory framework as well as in simplified models with vector mediators, using a multivariate analysis. For DM-quark effective operators with scalar, vector, and tensor couplings and DM mass of 100 GeV, the 5σ reach in the DM interaction scale Λ is around 2, 1, and 3 TeV, respectively, for 3 ab^{-1} and assuming a 5% systematic uncertainty on the total background normalization. For simplified models with leptophobic vector mediators, the 5σ reach for the mass of the mediator is 1.7 TeV also assuming a 5% systematics and 3 ab^{-1} of integrated luminosity. The reach for the dark matter interaction scale obtained with the multivariate analysis using a likelihood function discriminant is at least twice as high as that obtained from a simple cut and count analysis, once systematics on the background normalization larger than a few percent are taken into account. Moreover, the reach is much more stable against degradation due to these systematic uncertainties.

I. INTRODUCTION

The particle nature of dark matter (DM) is one of the most important unsolved questions in physics, and the focus of immense experimental and theoretical endeavors. One of the most promising arenas for such endeavors is the study of DM in colliders.

Approaches to study the dark matter parameter space include effective operators [1] and simplified models [2], with a mono-X observational signature, where X may denote jet [3], photon [4], Z [5, 6], W [7], Higgs [8], b [9], or top [9]. In studies with effective operators, limits on the cut-off scale Λ of the low energy DM effective field theory have been reported.

The purpose of the current paper is to explore the reach at 13 TeV for the effective interaction scale between DM and quarks as well as electroweak bosons. Moreover, we also study simplified models with DM-quark interactions mediated by leptophobic vector mediators. We explore the mass reach for such mediators. We choose the mono-Z channel for our study, since, compared to monojet, it is expected that background uncertainties should scale more favorably for the mono-Z signature. In mono-Z studies, a pair of charged leptons that reconstruct to a Z boson recoil against the missing transverse momentum carried by dark matter. The dominant background in this case is constituted by SM processes $ZZ \to \ell\ell\nu\nu$. Using ATLAS bounds on $ZZ \to \ell\ell\nu\nu$ [10], constraints were put on the dark matter effective scale Λ in [6].

We will be especially careful to incorporate the effects of systematic uncertainties, which are expected to become increasingly important in the current run of the LHC. Our strategy is to obtain a set of kinematic variables that can discriminate between signal and background, and construct a multivariate likelihood function on which cuts can be imposed. Broadly, we find that the reach for the DM interaction scale Λ obtained with the multivariate analysis using a likelihood function is at least twice as high as that obtained from a simple cut and count analysis, when systematic uncertainties greater than a few percent are taken into account. Moreover, the reach is much more stable against degradation due to systematics in the total background normalization.

The rest of the paper is structured as follows. In Section II, we first discuss both DM effective operators and simplified models with vector mediators. In Section III, we discuss the kinematic variables used in the construction of the multivariate discriminant. In Section IV, we discuss systematic uncertainties. In Section V, we discuss the construction of the multivariate (MVA) discriminant. In Section VI, we present the main results of our multivariate study for the DM effective operators, while in Section VII, we present the results for the Z' model. We end with our conclusions.

II. BACKGROUND: EFFECTIVE OPERATORS AND VECTOR MEDIATORS

In this Section, we describe the theoretical background of our study. We first discuss DM effective operators, and then turn to simplified models with vector mediators.

A. Effective Operators

Effective field theories for dark matter interacting primarily with SM quarks have been considered in Refs. [1, 3, 11–18].

We consider the following interactions

$$\sum_q \left\{ \frac{1}{\Lambda_{\tilde{D}1}^2} \bar{q}q \ \bar{\chi}\chi + \frac{1}{\Lambda_{D8}^2} \bar{q}\gamma^\mu\gamma_5 q \ \bar{\chi}\gamma_\mu\gamma_5\chi \right.$$
$$\left. + \frac{1}{\Lambda_{D5}^2} \bar{q}\gamma^\mu q \ \bar{\chi}\gamma_\mu\chi + \frac{1}{\Lambda_{D9}^2} \bar{q}\sigma^{\mu\nu} q \ \bar{\chi}\sigma_{\mu\nu}\chi \right\} \tag{1}$$

In the above, χ denotes a Dirac fermion that we assume to be the DM particle. We follow the naming conventions of [1]. The SM quarks are denoted by q. $\tilde{D}1$, D5, D8, and D9 denote effective DM-q operators with scalar, vector, axial-vector, and tensor couplings. These operators are chosen because they lead to a non-vanishing scattering rate with nucleons at small momentum transfer.

To simplify the analysis, we will assume that only one type of operator is dominant at one time, with the others decoupled. For the scalar operator $\tilde{D}1$ we assume an underlying model with a scalar mediator S with

democratic couplings to all quark flavors. A Higgs portal model, on the other hand, leads to quark mass suppressed couplings which cannot be probed by the LHC.

We also consider two operators studied in [6]

$$L_5 \equiv \frac{1}{\Lambda_5^3} \overline{\chi}\chi (D_\mu H)^\dagger D^\mu H \tag{2}$$

which arises at dimension 5, and

$$L_7 \equiv \frac{1}{\Lambda_7^3} \overline{\chi}\chi \sum_i k_1 F_i^{\mu\nu} F_{\mu\nu}^i \ , \tag{3}$$

which arises at dimension 7. Here, F_i with $i = 1, 2, 3$ are the field strengths for the SM gauge groups.

In [6], the CLs method was used to put limits on the cross section for new physics (and hence the scales Λ for the different operators) based on existing ATLAS results. An upper limit on the number of events coming from new physics was obtained from the expected number of background events with uncertainties. The 90% CL exclusion bounds on the scales Λ were given with 7 TeV data, and it was found that for some types of operators, scales of the order of 100 GeV - 1 TeV could be probed.

B. Vector Mediators

We now turn to simplified models with a leptophobic vector mediator. The Lagrangian is

$$\mathcal{L} = -\frac{g}{2c_W} \left[\sum_i g_f \bar{q}_i \gamma^\mu (1 - \gamma_5) q_i Z'_\mu + g_\chi \bar{\chi} \gamma^\mu (1 - \gamma_5) \chi \right] Z'_\mu \ , \tag{4}$$

where the q_i are SM quarks, g_f and g_χ parametrize the coupling between quarks and the vector mediator Z', and between the DM candidate χ and the Z', respectively, in terms of the SM coupling $\frac{g}{2c_W} = \frac{m_Z}{v} \sim 0.37$, where g is the $SU(2)_L$ coupling and c_W is the cosine of the Weinberg angle. In our simulations we choose $g_f = g_\chi = 1$ and $m_\chi = 100$ GeV as a benchmark point.

For this benchmark point, the branching ratios of a 500 GeV Z' to dark matter, jets and top quark pairs are 5.2%, 80.2% and 14.7%, respectively, and remain unchanged for larger masses. The ratio of the total width to $m_{Z'}$ is less than 0.1 for masses up to 4 TeV.

Collider studies of the Z' model have been performed by many authors in recent years, starting from the work of [15]. Bounds from direct and indirect dark matter detection and from colliders for a leptophobic Z' portal model were derived in [19], [20]. Overall, for couplings of SM size and a 100 GeV DM, strong bounds from LUX and dijet searches at the LHC 8TeV exclude a Z' portal up to $m_{Z'} \sim 2.8$ TeV. However, these bounds drop to $m_{Z'} \sim 2$ TeV for a 50% suppressed couplings to quarks or heavier DM. On the other hand, the branching ratio of the Z' to DM is mildly dependent on m_χ until it gets very close to the decay threshold, but increases very fast as the couplings between Z' and quarks get smaller. As a result, for a 500 GeV dark matter and 50% suppressed couplings to quarks, an 1 TeV Z', for example, is not excluded by any experiment and is able to reproduce the observed DM relic density [19].

III.   KINEMATIC VARIABLES FOR MULTIVARIATE ANALYSIS

In this Section, we describe the kinematic variables that will be used in our multivariate analysis. In the construction of a discriminant with a higher performance level than simple event counting, at least in certain regions of phase space, the information from the shape of the kinematic distributions is crucial. Combining this information in a likelihood function is one of the most simple, robust and straightforward means to build a multivariate discriminant between signal and background events.

In order to discriminate a dark matter signal at the LHC, we study the process

$$pp \rightarrow Z(\rightarrow \ell^+ \ell^-) \chi \overline{\chi} \ , \tag{5}$$

TABLE I. Production cross sections (in fb) for pair production of DM in association with a Z boson and one extra QCD jet at LHC 13 TeV: $pp \rightarrow Z\chi\bar{\chi} + j$. In the left part of the table we display the rates for the EFT operators considered in this work for $\Lambda_i = 1$ TeV as a function of the DM mass. In the right part, the rates for the leptophobic Z' model are given as a function of the Z' mass for $g_f = g_\chi = 1$ and $m_\chi = 100$ GeV.

m_χ (GeV)	$\tilde{\text{D}}1$	D5	D8	D9	Dim-5($\times 10^{-4}$)	Dim-7	$M_{Z'}$ (GeV)	Z'
≤ 10	275	47	47	1219	2.5	43	500	144
100	257	46	43	1204	1.2	39	1000	21.1
200	218	42	34	1058	0.59	31	2000	1.50
400	142	32	20	782	0.18	19	3000	0.18
1000	26	8	3	205	0.08	3	4000	0.03

where the DM χ interacts with quarks via operators $\tilde{\text{D}}1$, D5, D8, and D9 and directly with gauge bosons via operators L_5 and L_7. We also considered a process where dark matter is produced through the production and decay of a new leptophobic massive gauge boson Z'

$$pp \rightarrow Z(\rightarrow \ell^+\ell^-)Z'(\rightarrow \chi\bar{\chi}) . \tag{6}$$

The DM effective operators and the Z' simplified model were implemented in `FeynRules` [21]. Signal and background samples for $\ell^+\ell^- + \not{E}_T$ up to one extra jet are generated with `Madgraph` [22] followed by the parton showering and hadronization with `Pythia` [23] and the detector simulation using `Delphes` [24]. The hard (`MadGraph`) and soft jet (`Pythia`) regimes are matched according to the MLM [25] prescription at the matching scale $Q_{cut} = 20$ GeV for the EFT operators and 40 GeV for the heavy Z' bosons[1]. In Table (I) we display the production cross section for each operator for various dark matter masses keeping $\Lambda_i = 1$ TeV for 13 TeV LHC and for the Z' production and decay to dark matter in association to a SM Z boson keeping $g_f = g_\chi = 1$ and $m_\chi = 100$ GeV fixed. We note that the production cross section of the Dim-5 operator is suppressed, in agreement with previous studies [6].

The $ZZ \rightarrow \ell\ell\chi\bar{\chi}$ events are characterized by large $\not{E}_T$ and the presence of two high p_T isolated electrons or muons. The following preselection cuts were imposed, inspired by the ATLAS study of $ZZ \rightarrow \ell^+\ell^- + \not{E}_T$ [10]:

- two same-flavor opposite-sign electrons or muons, each with $p_T^\ell > 20$ GeV in $|\eta^\ell| < 2.5$ and dilepton invariant mass close to the Z boson mass: $m_{\ell\ell} \in [76, 106]$ GeV; $\Delta R_{\ell\ell} > 0.3$

- veto jets with $p_T^j > 25$ GeV and $|\eta^j| < 4.5$.

We also investigated an event selection without imposing the jet veto but keeping the p_T, η, and $m_{\ell\ell}$ requirements.

At the 13 TeV LHC, the dominant SM backgrounds after the Z window selection consists of $ZZ + j$ and $t\bar{t}$ events, with a sub-dominant contribution from $WW, Wt, WZ, \tau^+\tau^-$. The Wt and $\tau^+\tau^-$ backgrounds are negligible after we demand a $\not{E}_T$ cut:

- $\not{E}_T > 100, 150, \cdots, 500$ GeV

We chose the following kinematic variables to better classify the signal and background events both in the EFT as well as the simplified Z' model frameworks:

- Missing energy $\not{E}_T$ is expected to be the kinematic variable that offers one of the best avenues of discerning signal and background. However, this variable is used as a cut variable in order to reduce the number of background events but not to build the likelihood functions. At the LHC, the transverse missing energy serves as a trigger to new physics and a cut on $\not{E}_T$ is always necessary. In any case, $\not{E}_T$ is correlated to other variables which we actually use to construct the multivariate discriminant of our signal models and the backgrounds.

---

[1] Although we do not use it in the curent work, we note that NLO cross sections for the signal have been computed at the parton level and implemented in MCFM by [26], and in `POWHEG` by [27].

- The product $\not{E}_T \times \cos\left(\Delta\phi(\vec{E}_T^{miss}, \vec{p}_T^Z)\right)$, where $\Delta\phi$ is the angle between the two dimensional vector $\vec{E}_T^{miss}$ and the transverse momentum $\vec{p}_T^Z$ of the Z boson candidate. This serves as a measure of axial-$\not{E}_T$, which is defined as the projection of $\vec{E}_T^{miss}$ along the direction opposite to the Z candidate [10]. This variable has a great potential to discern between the various DM operators as suggested in [6].

- The fractional p_T difference $|\not{E}_T - p_T^Z|/p_T^Z$ [10].

- The azimuthal separation of the two leptons $\Delta\phi(\ell^+, \ell^-)$.

- $\alpha_T = E_T(\ell_2)/M_T$, where E_{T2} is the transverse energy of the softest lepton of the $\ell^+\ell^-$ pair and $M_T = \sqrt{(E_{T1} + E_{T2})^2 - (p_{x1} + p_{x2})^2 - (p_{y1} + p_{y2})^2}$. This variable has been studied by [28].

- The angular variable $\cos(\theta^*)$ [29] where θ^* is defined as the boost invariant $\cos(\theta^*) = \tanh\left(\frac{\eta_{\ell^+} - \eta_{\ell^-}}{2}\right)$. In the case of sparticles production and decay to short chains, as slepton to leptons $+ \not{E}_T$ [29], or sbottoms to bottom jets $+ \not{E}_T$ [30], this variable is shown to be correlated to the production angle of the sparticles.

- The contransverse mass $MT_c = \sqrt{2\left(\vec{p}_{T_\ell} \cdot \vec{p}_{T_\ell} + p_{T_\ell} p_{T_\ell}\right)}$ [31].

- The angular variable $\cos(\theta_M)$ [32], the cosine of the angle between the leptons' direction of motion and the beam-axis in the centre of mass frame of the leptons. Compared to $\cos(\theta^*)$, $\cos(\theta_M)$ is not sensitive to smearing effects observed as $|\cos(\theta^*)| \sim 1$, which diminishes the discerning power of the θ^* variable in this region.

We now turn to a discussion of the normalized distributions of the above variables. In the upper left panel of Fig. (1) we show the $\not{E}_T$ distribution for the SM backgrounds (dashed lines) and EFT interactions (solid lines). The black, blue, red, and green solid lines show the distributions for $\tilde{D}1$, D5, D9, and the dim-7 operators. Not surprisingly, vector (D5) and vector-axial couplings (D8) (not shown in the figure but very similar to D5) have the closest resemblance to the ZZ background (black dashed). The other EFT interactions, in turn, show harder distributions. The other panels of Fig. (1) display those variables which are correlated to $\not{E}_T$. In the upper right panel, we show the variable α_T, while in the bottom left and right panels we show the axial-$\not{E}_T$ and contransverse mass MT_c, respectively. In these figures, the SM background is shaded in orange, while the solid black and blue lines denote operators $\tilde{D}1$ and D5, respectively, while dotted black and blue lines denote D9 and the dim-7 operators, respectively.

In the Fig. (2) we show the angular variables used in the construction of the multivariate discriminant after the selection cuts and a missing transverse cut $\not{E}_T > 150$ GeV. In the upper left panel we show the azimuthal angle between the leptons. This is more peaked to small values for EFT operators than the SM backgrounds, a consequence of harder missing transverse momentum of dark matter which makes the signal lepton pairs more collimated. In other words, the Z boson transverse momentum gets more correlated to the dark matter pair p_T as can be seen at the upper right panel where, again, the EFT interactions lead to smaller fractional p_T difference $|\not{E}_T - p_T^Z|/p_T^Z$ as compared to the backgrounds. For the $\cos(\theta^*)$ and $\cos(\theta_M)$ distributions we see basically the same effect of enhanced collimation of EFT interactions compared to the SM events.

As a general remark we note that the vector effective interaction is, again, the most similar to the SM backgrounds (as well as D8), while $\tilde{D}1$, D9 and Dim-7 are similar to each other but less similar to the backgrounds. Of course, these features will have an impact on the discerning power of the discriminants for each EFT operator.

Demanding harder $\not{E}_T$ cuts to further separate signal events from backgrounds has a deleterious effect on the discrimination power of the shapes of these distributions. As $\not{E}_T$ increases, the Z momentum gets more correlated to the momentum of the dark matter pair, and higher correlation translates into increased similarity between signal and backgrounds distributions. This can be seen in Fig. (3) where we show, from left to right, the impact of increasing the $\not{E}_T$ cut on the $\Delta\phi(\ell^+, \ell^-)$ variable.

IV. SYSTEMATIC UNCERTAINTIES AND STATISTICAL SIGNIFICANCE

Systematic uncertainties frequently limit the reach of experiments, mainly in processes with small signal to background ratio. Multivariate techniques can be used to overcome these limits, extracting more information
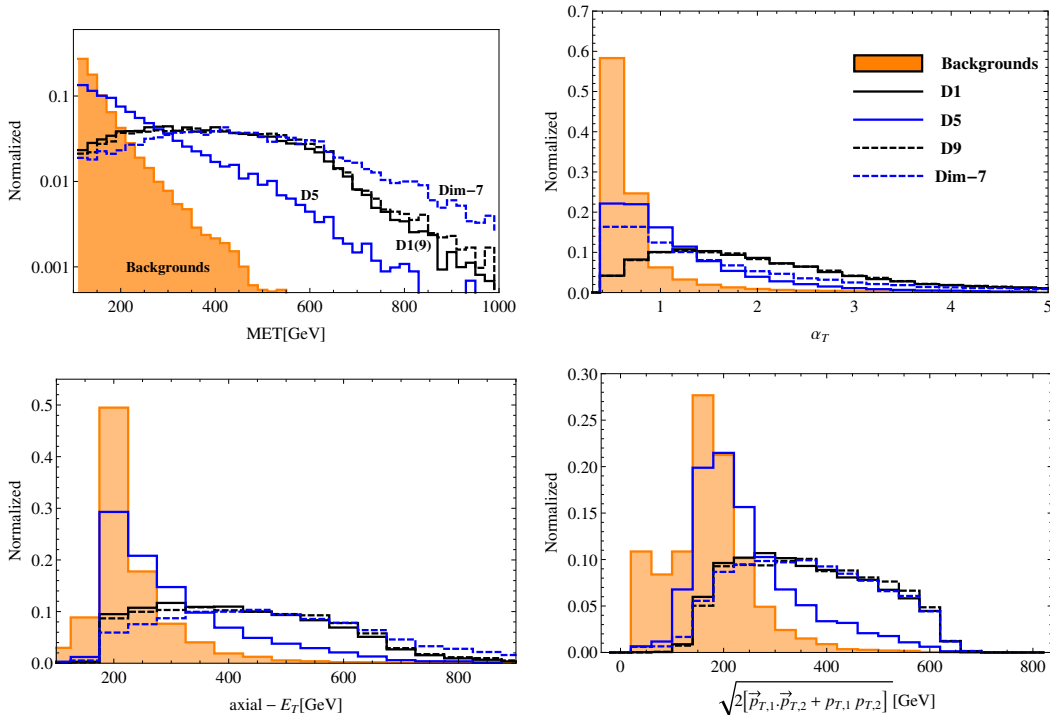
FIG. 1. Upper panel: Plot of $\not{E}_T$ (left) and α_T (right). Lower panel: Plot of $\not{E}_T \times \cos\left(\Delta\phi(\vec{p}_T^{\,miss}, \vec{p}_T^Z)\right)$ (left), and MT_c (right). Legend - upper left plot: Operator D1 (black solid line), operator D5 (blue solid line), operator D9 (red solid line), operator $ZZ\chi\chi$-dim 7 (green solid line). SM backgrounds are dashed, with $ZZ \to \ell\ell\nu\nu$ denoted by the black dashed line. Other plots: Operator D1 (black solid line), operator D5 (blue solid line), operator D9 (dotted black line), operator $ZZ\chi\chi$-dim 7 (dotted blue line), SM background (shaded orange).

and circumventing the constraints imposed by systematics in the statistical significance of a signal. A very good example is the single top measurement first observed by the CDF collaboration [33] where the combination of four multivariate techniques was necessary to extract the signal in spite of the small signal to background ratio and a large number of sources of systematic uncertainties.

Incorporating systematic uncertainties in the computation of the statistical significance level of a signal can be done in many ways and the subject itself has been debated in the statistical community [34].

There are many sources of systematics in a real experiment and taking all of them into account in a simulation is difficult. However, in a discovery analysis, the loss of statistical significance is, roughly, an effect of the widening of the probability density distribution of the chosen test statistic associated to the background hypothesis due to the presence of the systematic uncertainties. This can be more easily understood in terms of the naive significance metric given by

$$Z_{sb} = \frac{S}{\sqrt{B + (\varepsilon_{sys}B)^2}} \tag{7}$$

where S is the number of signal events, B the number of backgrounds events, and $\varepsilon_{sys}B$ the systematic uncertainty on the backgrounds in the limit of high statistics i.e. $B \gg 1$.

It is easy to invert this relation to obtain the minimum integrated luminosity required to reach a given statistical significance Z_{sb}. If σ_S and σ_B are the signal and backgrounds cross sections, respectively, it can be shown that $\sigma_S/\sigma_B > Z_{sb}\varepsilon_{sys}$ is a constraint on the achievable significance. If systematics are too large, a 5σ discovery, for example, is not possible no matter how much data has been accumulated.

The formula (7) given above takes into account only the total number of signal and background events and increasing the signal to background ratio can be done only in a cut-and-count analysis. This is our approach in this work, constructing a distribution where signal and backgrounds events are well separated and imposing a cut to clean up the signal events more efficiently than the $\not{E}_T$ distribution.
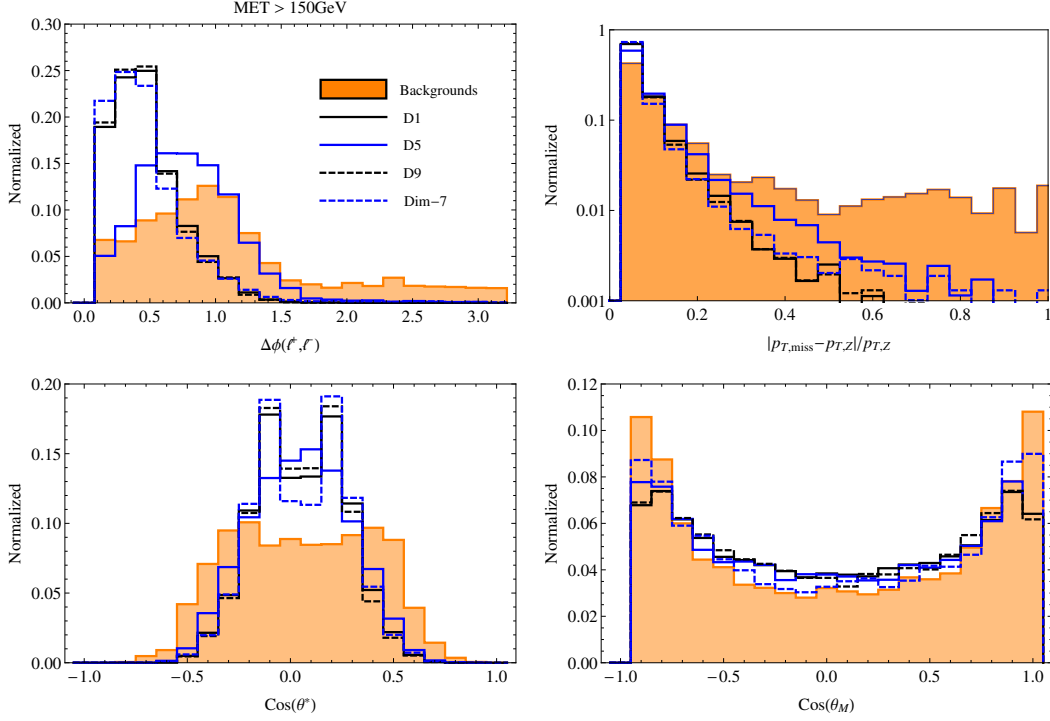
FIG. 2. Upper panel: Plot of $\Delta\phi(\ell^+, \ell^-)$ (left) and $|\not{E}_T - p_T^Z|/p_T^Z$ (right). Lower panel: $\cos(\theta^*)$ (left) and $\cos(\theta_M)$ (right). Legend: Operator D1 (black solid line), operator D5 (blue solid line), operator D9 (dotted black line), operator $ZZ\chi\chi$-dim 7 (dotted blue line), SM background (shaded orange).

Systematic uncertainties in the shape of the distributions used in the multivariate analysis might also be important, but that is beyond the scope of our work. We note that the results obtained in our more simple approach to systematics are sufficient to show that taking these errors into account is crucial to reliably estimate the reach of the experiment.

For the purpose of calculating the signal significance in the presence of systematic uncertainties in the number of backgrounds events we use, instead of Eq. (7) which is shown to overestimate the significance for $\varepsilon_{sys} < 1$ [34], the metric proposed in [35], Z_{PL}, which is simple to use and is shown to be an excellent approximation to the consistent frequentist computation using Poisson distributions. Moreover, we found that among the three more reliable methods to compute the statistical significance incorporating systematic uncertainties, Z_{PL} is the most conservative one. More details on these metrics are given in Appendix A.
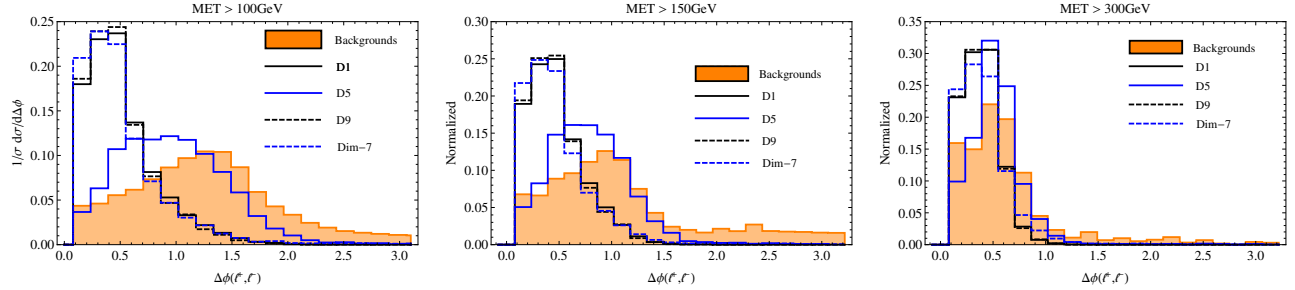

FIG. 3. From left to right, the impact of increasing the $\not{E}_T$ cut ($\not{E}_T > 100,\ 150,\ $ and 300 GeV, respectively) on the $\Delta\phi(\ell^+, \ell^-)$ variable.

The background estimation and signal extraction strategies would depend on upgraded detector designs and trigger conditions, especially in high pileup conditions. However, based on current data, we can give a

very simple estimation of the systematic uncertainties on the $ZZ \to \ell\ell\nu\nu$ background. In [10], the ATLAS collaboration studied the process $ZZ \to \ell\ell\nu\nu$ at 7 TeV with 4.6 fb^{-1} of data, with an event count of $39.3 \pm 0.4 \pm 3.7$, where the first and second uncertainties are statistical and systematic, respectively. The systematic uncertainties include contributions from uncertainties in the lepton reconstruction efficiency and the lepton energy scale and resolution, the missing transverse energy modeling, the jet veto uncertainty and uncertainties in the trigger efficiency, PDF and scale, and generator modeling and parton shower. In a recent study from the CMS collaboration, [36], the cross section for the process $pp \to ZZ \to \ell\ell\nu\nu$ was given as $88^{+11}_{-10}(stat)^{+24}_{-18}(syst)$ fb at 8 TeV with Z bosons in the mass range 60 to 120 GeV. From the above estimates, it is clear that systematic uncertainties $\sim \mathcal{O}(10\%)$ are possible. The systematic uncertainties at 13 TeV are conservatively expected to be of the same order, although a 13 TeV study for the process $pp \to ZZ \to \ell\ell\nu\nu$ has not been published by the collaborations yet.

The other SM background that is important besides $ZZ + j$ includes contributions from $t\bar{t}, WW, WZ$. However, as we are going to show, after applying the MVA and jet veto selections they become negligible and the only relevant sources of systematic errors are those associated to the ZZ backgrounds as we described here.

V. MULTIVARIATE ANALYSIS AND RESULTS

One robust method for combining several sensitive variables is the multivariate likelihood function [33, 37–39], a Bayesian learning classifier [40]. The relative probabilities of finding an event in histograms of each input variable described above is used, comparing between signal and background.

Binned probability density functions for each input variable are used to construct the likelihood function $\mathcal{D}_k$, where k denotes the event class ($k = 1$ for signal, $k = 2, 3, 4, 5$ for ZZ, WW, ZW and $t\bar{t}$ backgrounds, respectively). We denote by f_{ijk} the probability that an event from the sample k will populate the bin j of the kinematic variable i. The probabilities are normalized to

$$\sum_j f_{ijk} = 1 \tag{8}$$

for every variable i and event sample k. The likelihood function is computed as follows. For each reconstructed variable i, the bin j in which the event falls is obtained. The quantities

$$p_{ik} = \frac{f_{ijk}}{\sum_{m=1}^{5} f_{ijm}} \tag{9}$$

are computed for every variable i and all values of k. These quantities p_{ik} are finally used to calculate the likelihood function

$$\mathcal{D}_k = \frac{\prod_{i=1}^{n_{var}} p_{ik}}{\sum_{m=1}^{5} \prod_{i=1}^{n_{var}} p_{im}} \tag{10}$$

where n_{var} is the number of input variables. The quantity $\mathcal{D}_{LF} \equiv \mathcal{D}_1$, corresponding to the signal likelihood function, is referred to as the likelihood discriminant.

We note that the likelihood function does not use correlations between the variables, although since the distributions are obtained from the fully simulated Monte Carlo data, any correlations are included in the modeling. More sophisticated analyses take advantage of the correlations between the variables.

In Fig. (4), we display the likelihood function $\mathcal{D}_{LF}$ distributions for operators $\tilde{\text{D}}1$, D5 (D8 is very similar to D5), D9, dim-5, and dim-7 after cuts on $\not{E}_T$ have been applied. The blue line shows the distribution for signal, while the red line shows the distribution for background. It is clear that the signal peaks near $\mathcal{D}_{LF} = 1$, while the background peaks near $\mathcal{D}_{LF} = 0$. Nevertheless, we observe smaller signal peaks in the background region, where the likelihood discriminant classified signal events as background events, and *vice-versa*. This can be understood if one keeps in mind that leptons from both the signal and the dominant background ZZ are the yields of a Z boson decay, and thus it is natural that a fraction of signal events are misidentified as background events. The most distinctive features of the kinematic variables are driven by the dark matter interactions and the identity of the source of missing energy - the neutrinos in the SM case, and the χ DM in the case of new physics parametrized by the EFT operators.
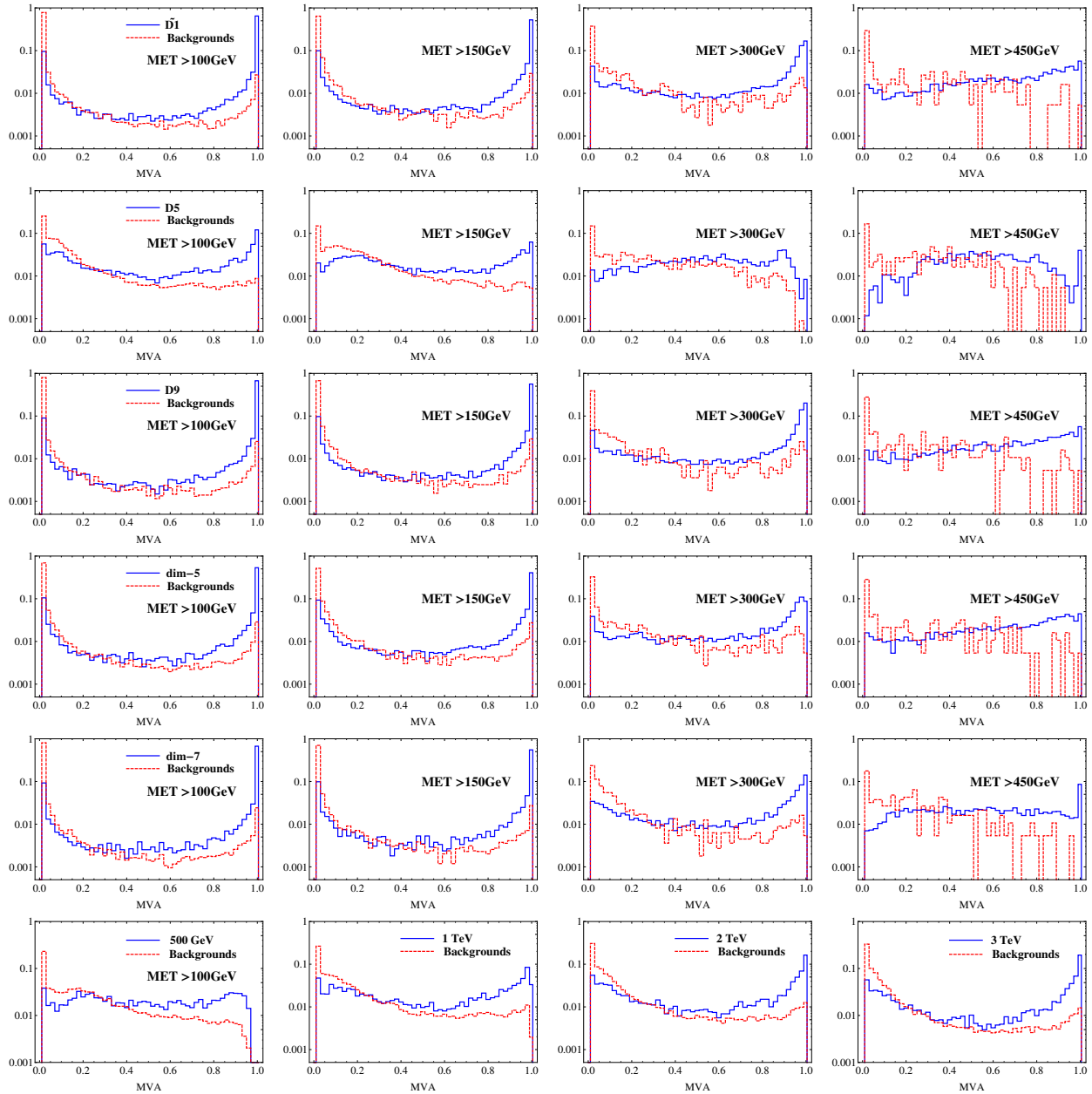
FIG. 4. The likelihood function $\mathcal{D}_{LF}$ is displayed for operators $\tilde{D}1$, D5, D9, dim-5, dim-7, and the Z' model. The blue line shows the distribution for signal, while the red line shows the distribution for background. The EFT plots show the effect of the $\not{E}_T$ cut on the discerning power of the likelihood discriminant, while the Z' plots, at the lowest row, show that heavier Z' are easier to separate from the SM backgrounds. For Z' we fixed $\not{E}_T > 100$ GeV.

A harder $\not{E}_T$ cut results in EFT signal and background distributions for the likelihood function that look similar. This happens due to the fact that the signal and background shapes of the kinematic distributions start to become similar as the $\not{E}_T$ cut is increased as we have shown in Fig. (3). To obtain optimal reach, one thus has to balance between the $\not{E}_T$ cut and the cut on $\mathcal{D}_{LF}$. The $\not{E}_T$ cut is chosen to be $\not{E}_T > 100, 150, 300$ and 450 GeV. It is clear that increasing the $\not{E}_T$ cut gradually makes the signal and background distributions of $\mathcal{D}_{LF}$ similar, reducing the efficiency of the $\mathcal{D}_{LF}$ cut. The same behavior concerning $\not{E}_T$ cuts were observed in the case of Z' events. The reason for choosing the benchmark lowest value of $\not{E}_T$ cut 100 GeV was for compatibility with triggers. It is possible that going a bit lower in $\not{E}_T$ can be of some advantage, although even

at this value the likelihood function $\mathcal{D}_{LF}$ is peaking quite clearly near 1 (0) for signal (background).

At the lowest row of Fig. (4) we show the likelihood distributions for the Z' model for $M_{Z'} = 0.5$, 1, 2 and 3 TeV fixing $\not{E}_T > 100$ GeV. In this case, $\mathcal{D}_{LF}$ performs better for heavier Z'. This is expected, since a lighter Z' tends to look like a SM Z boson, that is, the ZZ' process become less distinguishable from the ZZ, in spite of the fact that $\not{E}_T$ is due a heavy DM in the signal case. Compared to EFT operators, the Z' discriminant distributions discern better signal from backgrounds.
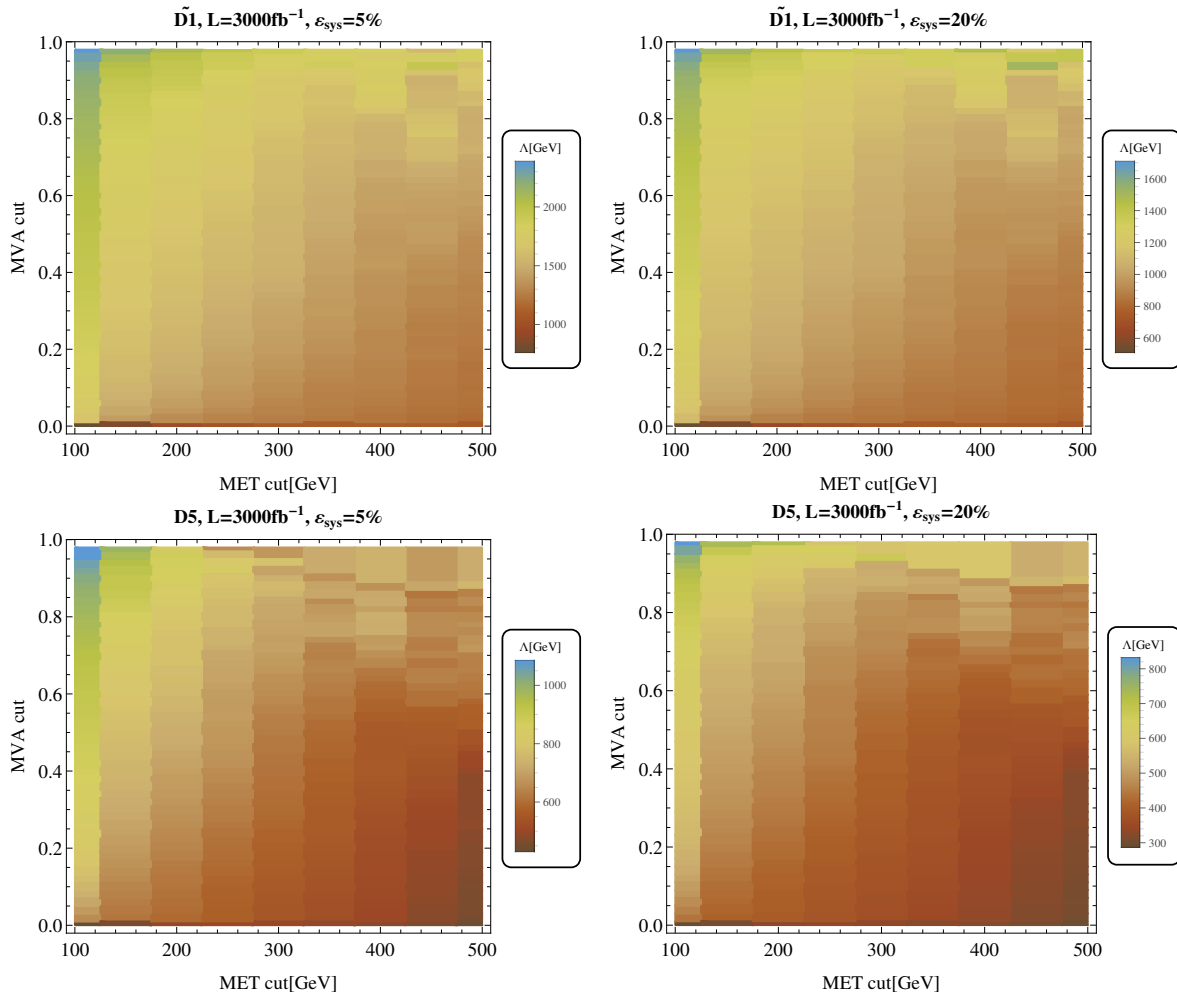

FIG. 5. The reach(5σ) for the cut-off scale Λ is shown at the upper and middle rows for various choices of cuts on $\mathcal{D}_{LF}$ (vertical axis) and $\not{E}_T$ (horizontal axis), for 3 ab^{-1} of integrated luminosity. At the upper row we show the results for the $\tilde{D}1$ operator, while at the middle row results for the D5 operator are shown.

In the next Section, we go on to give our main results for the EFT operators.

VI. RESULTS FOR EFT OPERATORS

As described previously, the discovery reach (5σ) for Λ depends on a judicious choice of $\not{E}_T$ cut and a cut on the likelihood function $\mathcal{D}_{LF}$. We display the reach for a variety of luminosities and choices of systematics. The results for the operator $\tilde{D}1$, with a jeto veto, are shown in the upper row of Fig. 5. The reach for the cut-off scale Λ is shown for various choices of cuts on $\mathcal{D}_{LF}$ (vertical axis) and $\not{E}_T$ (horizontal axis), for different luminosities and systematics. The reach for luminosity 300 fb^{-1}, for systematics of 5% (20%), is 1857 (1500) GeV. The reach for luminosity 3000 fb^{-1}, for systematics of 5% (20%), is 2209 (1542) GeV. As is clear from
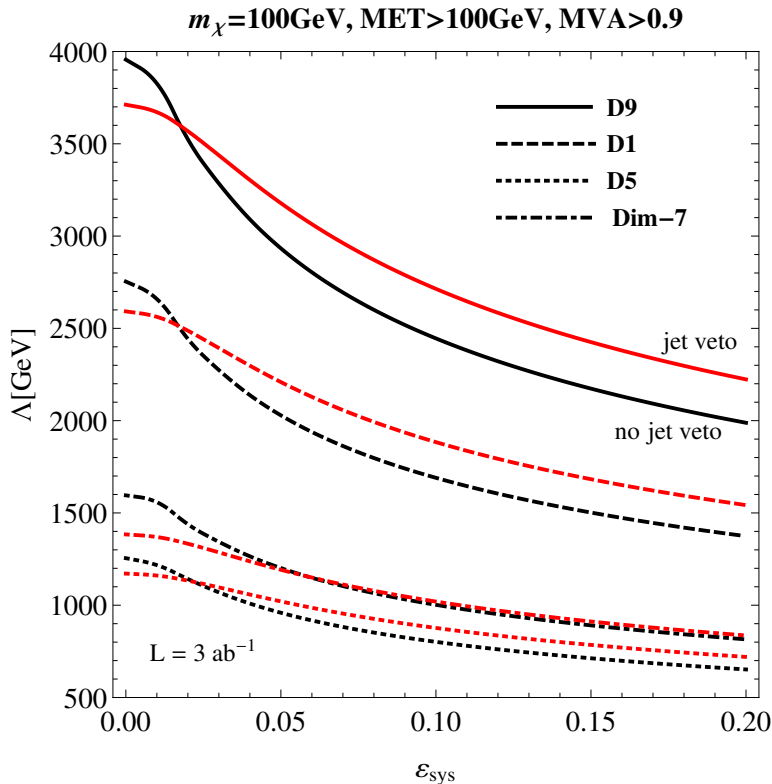
FIG. 6. **Reach in Λ for EFT operators**: The reach in Λ for the EFT operators at 3000 fb^{-1} of integrated luminosity. The red curves display the case when jet veto is applied, while the black curves display the case when no jet veto is applied. The mass of the DM candidate is fixed at 100 GeV. The cuts applied are $\not{E}_T > 100$ GeV and $\mathcal{D}_{LF} > 0.9$.

the figure, the maximum reach is obtained for $\not{E}_T > 100$ GeV, $\mathcal{D}_{LF} > 0.9$. We observed very similar behavior concerning operators D9, dim-5 and dim-7. The reach for the dim-5 operator is limited to a few tens of GeV even for low systematics and high luminosities. We summarize in Table (II) the results for all operators but dim-5.

The results for the operator D5 are shown in the middle row of Fig. 5. The results for operator D8 are similar. The reach for luminosity 300 fb^{-1}, for systematics of 5% (20%), is 843 (695) GeV. The reach for luminosity 3000 fb^{-1}, for systematics of 5% (20%), is 1021 (720) GeV. In this case, however, we see that a harder $\not{E}_T$ cut degrades the achievable reach of the LHC compared to the other operators. This is, again, due the larger similarity between the shapes of the kinematic distributions of D5 (and D8) operator and the backgrounds as can be seen in Figs. (1), (2) and (3).

The final results at 3000 fb^{-1} for the reach in Λ for all the EFT operators are displayed in Fig. 6. The reach in Λ for the EFT operators is shown at 3000 fb^{-1} of integrated luminosity. The red curves display the case when a jet veto is applied, while the black curves display the case when no jet veto is required. The mass of the DM candidate is fixed at 100 GeV throughout all our analyses. The cuts applied are $\not{E}_T > 100$ GeV and $\mathcal{D}_{LF} > 0.9$. The solid, long-dashed, short-dashed, and dot-dashed curves denote the limits for D9, $\tilde{D}1$, D5, and the dim-7 operators, respectively. The D8 curves are very close to the D5 ones.

First of all, we see that including systematic uncertainties is a really necessary ingredient to get realistic estimates for the reach of the LHC for dark matter. Keeping systematics under control might improve the reach discovery by a factor of two roughly. For example, in the D9 case, a 20% systematics in the backgrounds reduces the reach to ~ 2200 GeV, while keeping a 5% level or less increases the reach to ~ 3500 GeV or farthest.

Adopting a jet veto also helps to get a larger reach for dark matter searches in the mono-Z channel if the systematics are larger than approximately 3-5%.

TABLE II. Results for EFT operators and the leptophobic dark Z' portal for three different selection cuts, integrated luminosities of 0.3 and 3 ab^{-1}, and systematic uncertainties of 5% and 20% in the total background rate. The last row shows the effect of including a jet veto in the analysis. The blank entries in the last column indicate that a 5σ discovery cannot be reached for that luminosity and level of systematics.

CUTS	L(ab^{-1})	sys(%)	$\tilde{D}1$	D5	D8	D9	Dim-7	$M_{Z'}$
$\not{E}_T > 100$ GeV	0.3	5	702	404	398	994	400	327
		20	470	270	266	665	268	–
	3	5	702	404	398	996	401	328
		20	470	270	266	666	268	–
$\not{E}_T > 100$ GeV $+ \mathcal{D}_{LF} > 0.9$	0.3	5	1864	868	859	2686	1096	675
		20	1363	645	635	1972	808	675
	3	5	2030	959	859	2944	1201	1690
		20	1374	652	635	1988	815	1010
$\not{E}_T > 100$ GeV $+ \mathcal{D}_{LF} > 0.9$ + jet veto	0.3	5	1857	843	835	2663	994	1233
		20	1500	695	684	2159	810	906
	3	5	2209	1021	1005	3178	1192	1485
		20	1542	720	707	2224	836	937

A. Comparative Performances of $\mathcal{D}_{LF}$ and $\not{E}_T$ Cut for EFT Operators
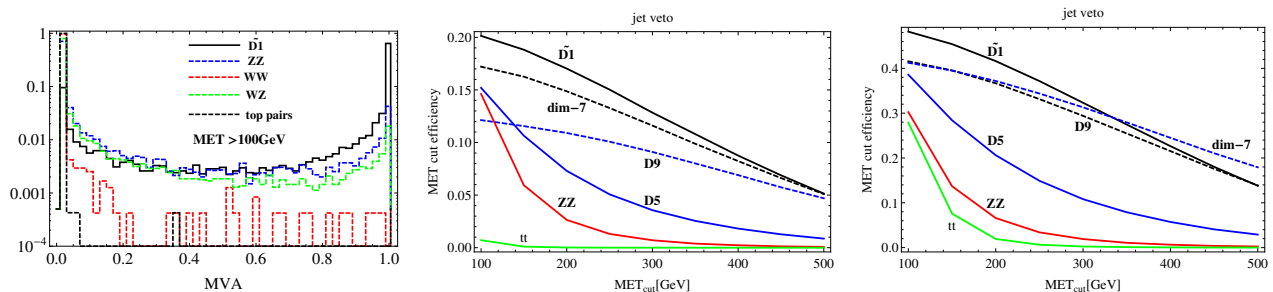

FIG. 7. In the left panel, the $\mathcal{D}_{LF}$ discriminant distribution for the $\tilde{D}1$ operator (solid line) and all the relevant backgrounds (dashed lines) for a mono-Z search. In the central(right) panel we display the cut efficiency with just a $\not{E}_T$ cut of 100 GeV with(without) a jet veto for all the EFT operators, but dim-5, and for ZZ and top pair backgrounds.

The sensitivity to systematic uncertainties decreases with a higher cut on $\mathcal{D}_{LF}$, which results in a larger S/B ratio. We checked that the signal to background ratio increases of an order of magnitude after imposing $\mathcal{D}_{LF} > 0.8$ compared to the $\not{E}_T$ cut analysis alone, for all $\not{E}_T$ cuts, reaching $S/B \sim 7$ for a 100 GeV $\not{E}_T$ cut and $\mathcal{D}_{LF} > 0.9$ with and without a jet veto.

In the 13 TeV LHC, top quark pair production is not as harmless as in 7 or 8 TeV runs concerning the mono-Z channel. In this respect the combination of a $\mathcal{D}_{LF}$ discriminant and a jet veto can be used to eliminate background events not involving a SM Z boson. This can be seen in Fig. (7). First, in the left panel, note that the $\mathcal{D}_{LF}$ distributions of $t\bar{t}$ and WW backgrounds are highly concentrated near $\mathcal{D}_{LF} = 0$, while those ZZ and ZW are more widely distributed. Demanding $\mathcal{D}_{LF} > 0.5$ gets rid of all top events and the majority of WW backgrounds. In the central(right) panel we show the cut efficiency for a $\not{E}_T$ cut only with(without) the jet veto for $\tilde{D}1$, D5, D9, and dim-7 operators, and the ZZ and top pair backgrounds. Again, the top backgrounds can be more efficiently eliminated by tagging the hard bottom jets from top decays.

Let us discuss the advantage of using the multivariate analysis that we have described, when compared to a simple $\not{E}_T$ cut. In Fig. 8, we show the ratio of the reach in Λ when the $\not{E}_T$ cut is combined with $\mathcal{D}_{LF}$, compared to when only the $\not{E}_T$ cut is applied. With no systematics, the reach in Λ with $\mathcal{D}_{LF}$ is approximately $1.2 - 1.4$ times larger than the case with only $\not{E}_T$ cut. This ratio increases dramatically with increasing systematics, reaching $2.0 - 2.4$ for $\sim 5\%$ systematics, after which it becomes stable for a wide range of integrated luminosities from 300 to 3000 fb^{-1}. This clearly shows the advantage of using the $\mathcal{D}_{LF}$ for realistic systematics.
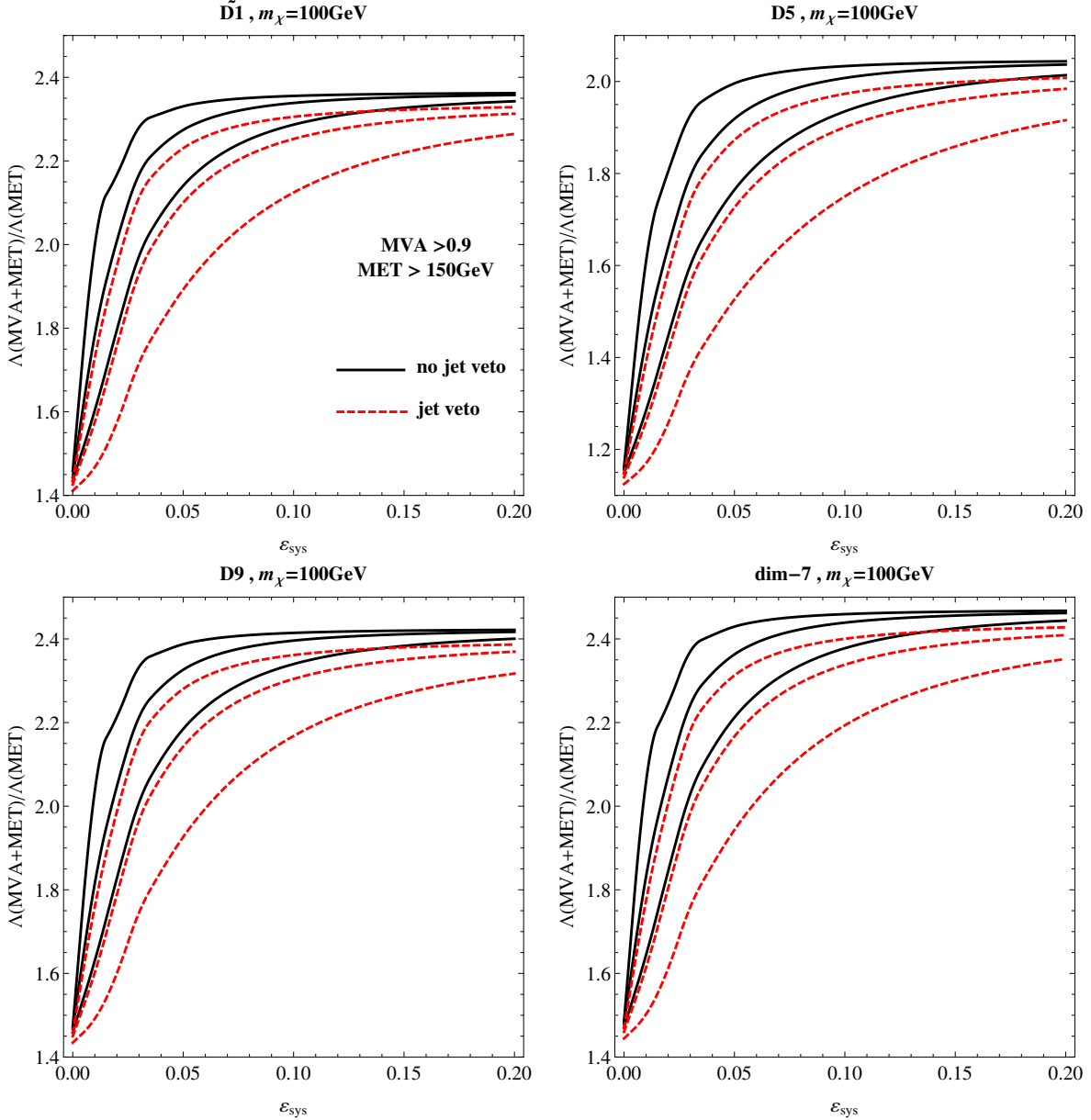
FIG. 8. The ratio of the reach in Λ, as a function of systematics, when the $\not{E}_T$ cut is combined with $\mathcal{D}_{LF}$, compared to when only the $\not{E}_T$ cut is applied, for $\tilde{D}1$, D5, D9, and dim-7 operators. The dashed(solid) lines show the ratios when we do(not) apply a jet veto. The lower red curves were obtained fixing the luminsoity at 300 fb^{-1}, the central blue ones at 1000 fb^{-1}, and the upper black curves at 3000 fb^{-1}.

VII. RESULTS FOR THE LEPTOPHOBIC DARK Z' PORTAL MODEL

Applying the multivariate analysis to the same kinematic observables in this case, we obtain the likelihood function for different masses of Z'. We will take $g_f = g_\chi = 1$ and $m_\chi = 100$ GeV in what follows.

In the last row of Fig.(5), the significance is shown for the mediator mass $m_{Z'} = 1$ TeV, for an integrated luminosity of 3 ab^{-1} and 5 and 20% systematics.

In Fig. 9, the upper row shows the statistical significance for the discovery of an 1 TeV Z' with couplings $g_f = g_\chi = 1$. The reach (5σ) for the cut-off scale Λ is shown for various choices of cuts on $\mathcal{D}_{LF}$ (vertical axis) and $\not{E}_T$ (horizontal axis), for 3 ab^{-1} of integrated luminosity. The left(right) panel shows results when
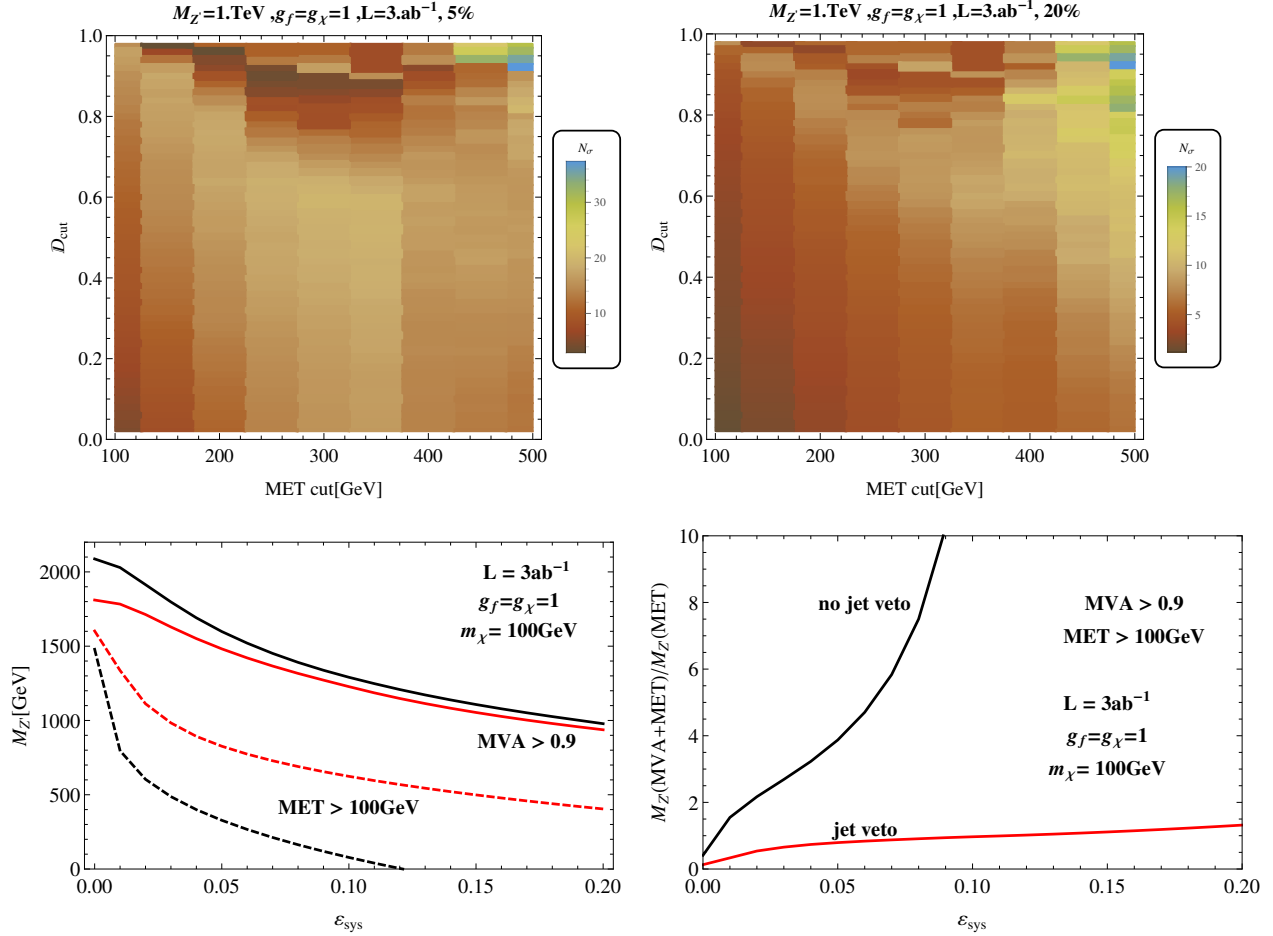
FIG. 9. **Reach in $M_{Z'}$**: Upper row: The statistical significance for the discovery of an 1 TeV Z' with couplings $g_f = g_\chi = 1$ is shown. The reach (5σ) for the cut-off scale Λ is shown for various choices of cuts on $\mathcal{D}_{LF}$ (vertical axis) and $\not{E}_T$ (horizontal axis), for 3 ab^{-1} of integrated luminosity. The left(right) panel shows results when the systematic uncertainty is 5(20)%. Lower row: At the left, the 5σ reach in M_Z' for $\not{E}_T > 100$ GeV cut only (dashed curves) and $\not{E}_T$ cut combined with the $\mathcal{D}_{LF} > 0.9$ cut on the likelihood function (solid curves), with a jet veto (red curves), and withou a jet veto (black curves), at 3000 fb^{-1} of integrated luminosity. The dark matter mass is fixed at 100 GeV and $g_\chi = g_f = 1$. At the right panel we show the gain in the 5σ discovery reach in terms of the Z' mass.

the systematic uncertainty is 5(20)%. The lower row shows the 5σ reach in m_Z' for $\not{E}_T > 100$ GeV cut only and $\not{E}_T$ cut combined with different cuts on the likelihood function $\mathcal{D}_{LF}$ are shown, at 3 ab^{-1} of integrated luminosity. It is clear from the results that for no systematics, the reach with $\mathcal{D}_{LF}$ is around 2 TeV, while the reach with $\not{E}_T$ cut is around 1.5 TeV. For increasing systematics, there is rapid degeneration of this reach for the case when only $\not{E}_T$ cut is used. For the $\mathcal{D}_{LF}$ analysis, the degeneration is much more gradual, and even for high systematics, the reach is still above 1 TeV.

Contrary to the case of EFT operators, imposing no jet veto on the events is advantageous for all systematics if we combine $\mathcal{D}_{LF}$ and $\not{E}_T$ cuts. However, for a $\not{E}_T$ cut alone, the reach is much more depleted in comparison to the jet veto case. A 5σ signal cannot be reached even for 3 ab^{-1} if $\varepsilon_{sys} > 0.12$ as we see in the left panel of Fig. (9). We conclude that a jet veto removes more signal and background events, but with a higher signal to background ratio.

At the right panel of Fig. (9) we show the gain in the 5σ reach, now in terms of the Z' mass, after applying the MVA cut with (solid red) and without a jet veto (solid black). In the case of a jet veto the gain is modest when the systematics are too small but increases as they get larger reaching almost a factor of 2 for $\varepsilon_{sys} \sim 0.2$. The no jet veto case by its turn shows a dramatic gain as the systematics approaches the 0.1 level. This is easy to understand if we take a look at the left panel of Fig. (9) and realize that for $\varepsilon_{sys} > 0.12$ it is impossible to

discover a Z'-like dark matter signal even with high statistics if we do not apply the MVA cut.

As in the case of EFT models, the sensitivity to systematics is greatly reduced when the $\mathcal{D}_{LF}$ discriminant is introduced and a cut is imposed on it, leading to higher S/B ratios. We also checked, for these Z' models, that the signal to background ratio increases of an order of magnitude after imposing $\mathcal{D}_{LF} > 0.8$ compared to the $\not{E}_T$ cut analysis alone without a jet veto.

VIII.   CONCLUSIONS

In this paper, we have investigated the discovery prospects of DM effective operators and simplified models with vector mediators at Run II of the LHC. We have paid particular attention to the question of systematic uncertainties. To that end, we have based our study on a multivariate analysis in the mono-Z channel.

Our main results are the following. We have seen that the reach obtained using a multivariate discriminant is typically at least twice as high as that obtained from a simple cut and count analysis, once systematic uncertainties in the total background normalization higher than a few percent are taken into account. This is clear from Fig. 8. With no systematics, the reach in Λ with the multivariate analysis is approximately $1.2 - 1.4$ times larger than the case with only $\not{E}_T$ cut. This ratio increases dramatically with increasing systematics, reaching $2.0 - 2.4$ for $\sim 5\%$ systematics, after which it becomes stable. This clearly shows the advantage of using the $\mathcal{D}_{LF}$ for realistic systematics.

Moreover, the reach is much more stable against degradation due to systematics, both for the EFT analysis as well as for the Z' analysis. This is clear from Fig. 9, where we show the results of the Z' analysis. For no systematics, the reach in $m_{Z'}$ with multivariate analysis is around 2 TeV, while the reach with only $\not{E}_T$ cut is around 1.5 TeV. For increasing systematics, there is rapid degeneration of the reach for the case when only $\not{E}_T$ cut is used. For the multivariate analysis, the degeneration is much more gradual, and even for high systematics, the reach is still above 1 TeV.

We also investigated the impact of including a jet veto to suppress backgrounds further. We found that a jet veto improves the reaches for the EFT as long as the level of systematics exceeds 3–5%. For the leptophobic Z' simplified model, requiring no jet veto provides better results when we perform the multivariate analysis, but it is important if just a $\not{E}_T$ cut is used.

Our reaches are the following. For DM-quark effective operators with scalar, vector, and tensor couplings and DM mass 100 GeV, the 5σ reaches in the DM interaction scale Λ keeping the level of systematics at 5% with 300 (3000) fb^{-1} of integrated luminosity are 1864 (2209) GeV, 959 (1021) GeV, and 2686 (3178) GeV, respectively. For simplified models with leptophobic vector mediators, the 5σ reach for the mass of the mediator is 1233 (1485) GeV with 5% systematics and 300 (3000) fb^{-1} of data.

IX.   ACKNOWLEDGMENTS

Appendix A: Details of the significance computation

A comprehensive study of various methods for the calculation of statistical significances has been presented in [34]. In this work, the problem of incorporating systematic uncertainties in the background normalization for a Poisson process is addressed and it is found that three most widely used significance metrics perform similarly in many situations concerning the relative number of signal and background events and the level of systematics. The three metrics are computed as follows:

$\underline{Z_{sb}}$ This is the naive and most simple way to incorporate systematic uncertainties in the calculation of the significances for S signal events and B background events in a Poisson process for a given integrated luminosity

$$Z_{sb} = \frac{S}{\sqrt{B + \sigma_{sys}^2}}$$

In all cases, we assume that the systematic uncertainty in the total background normalization is proportional to the number of background events, $\sigma_{sys} = \varepsilon_{sys}B$. This is simple and fast, but as in [34], we found it somewhat overestimates the reach as we show in Fig. (10), the upper blue lines.

$\underline{Z_N}$ The Bayesian-frequentist hybrid recipe to the estimation of the systematics impact on the significance. Assuming that systematic errors are normally distributed we marginalize over the systematic errors to obtain the p-value

$$p = \sum_{k=S+B}^{+\infty} \int_{-\infty}^{+\infty} \frac{e^{-B(1+z\varepsilon_{sys})}}{k!} \left[B(1 + z\varepsilon_{sys})\right]^k \times \frac{e^{-\frac{z^2}{2}}}{\sqrt{2\pi}} \, dz$$

and the significance is computed as $Z_N = \Phi^{-1}(1-p)$, where $\Phi(z)$ is the cumulative distribution function of the standard normal distribution.

This method demands a much larger computation effort. As we show in Fig. (10), the middle red lines, its performance is almost identical to the naive Z_{sb} metric though, despite the reach in Λ is always shorter than Z_{sb}. In the right panel we see that in the regime of a low number of events, Z_N might present numerical instabilities.

$\underline{Z_{PL}}$ The Profile Likelihood method originally proposed in [35] in astrophysical searches with subsidiary measurements of the background adapted to a high energy experiment where the systematics is a fraction of background events, $\sigma_{sys} = \varepsilon_{sys}B$

$$Z_{PL} = \sqrt{2} \left\{ (S+B) \ln \left[\left(1 + \frac{B}{\sigma_{sys}^2}\right) \frac{S+B}{S+B+B^2/\sigma_{sys}^2} \right] + \frac{B^2}{\sigma_{sys}^2} \left[\left(1 + \frac{\sigma_{sys}^2}{B}\right) \frac{B^2/\sigma_{sys}^2}{S+B+B^2/\sigma_{sys}^2} \right] \right\}^{\frac{1}{2}}$$

Among the three metrics this is the most conservative and reliable, and it is as simple and fast to compute as Z_{sb} [34]. Moreover, its performance is very close to the consistent frequentist approach for tests of the ratio of Poisson means implemented in `ROOT` [41], for example. The Z_{PL} results correspond to the lower black lines in Fig. (10).
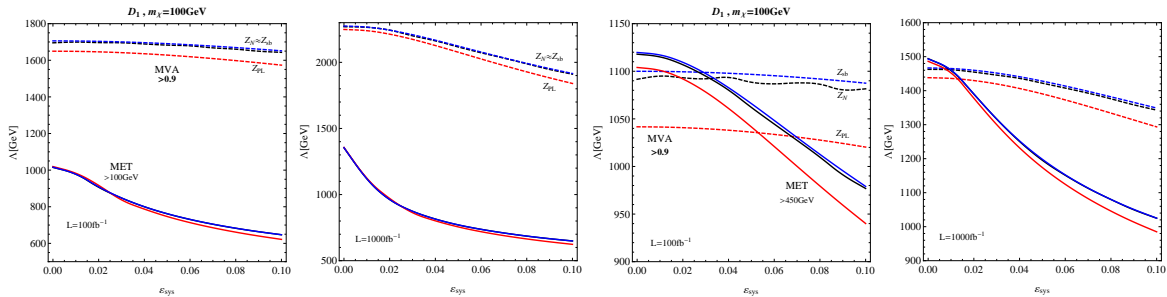

FIG. 10. Comparison of significance calculation methods. The solid(dashed) lines represent the reach in Λ for the scalar $\tilde{D}1$ operator for $m_\chi = 100$ GeV with $\not{E}_T$($\not{E}_T + \mathcal{D}_{LF}$) cuts as a function of the systematic uncertainties ε_{sys} for 100 and 1000 fb^{-1}. The upper, middle and lower dashed(solid) lines correspond to Z_{sb}, Z_N, and Z_{PL} metrics respectively. For solid lines we apply only a 100 GeV or 450 GeV $\not{E}_T$ cut, while for the dashed ones we also impose the $\mathcal{D}_{LF}$ cut $\mathcal{D}_{LF} > 0.9$.

In order to choose judiciously among these three significances metrics, a performance comparison for our benchmark point in the case of determining the LHC reach for the scalar operator $\tilde{D}1$ was carried out. In the Fig. (10) we show the reach in Λ using Z_{sb} (upper blue), Z_N (middle red), and Z_{PL} (lower black) in the multivariate analysis (dashed lines) and the simple cut-and-count analysis (solid lines). In the left(right) panels we assume a 100(1000) fb^{-1} of integrated luminosity for $\mathcal{D}_{LF} > 0.9$ and a $\slashed{E}_T$ cut of 100 GeV and 450 GeV.

The Profile Likelihood metric Z_{PL} is the most conservative one, thus confirming the findings of [34]. The reaches, however, are similar, especially comparing Z_{sb} and Z_N in the regime of a higher number of signal and background events. As the number of events decrease, as in the case of a hard $\slashed{E}_T$ cut of 450 GeV, the overestimation of Z_{sb} and Z_N gets more noticeable. Also, numerical instabilities appear in the computation of Z_N and a greater care is necessary when using this method.

Using the multivariate discriminant to better separate signal and backgrounds increases the S/B ratio compared to a simple $\slashed{E}_T$ cut. In this regime (dashed lines), Z_{sb} and Z_N also overestimate the reach compared to Z_{PL}, but the performances are very close with a $\slashed{E}_T$ cut only (solid lines), that is it, for smaller S/B ratios.

[1] J. Goodman, M. Ibe, A. Rajaraman, W. Shepherd, T. M. P. Tait and H. B. Yu, Phys. Rev. D **82**, 116010 (2010) [arXiv:1008.1783 [hep-ph]].

[2] J. Abdallah, A. Ashkenazi, A. Boveia, G. Busoni, A. De Simone, C. Doglioni, A. Efrati and E. Etzion *et al.*, arXiv:1409.2893 [hep-ph].

[3] M. Beltran, D. Hooper, E. W. Kolb, Z. A. C. Krusberg and T. M. P. Tait, JHEP **1009**, 037 (2010) [arXiv:1002.4137 [hep-ph]].

[4] Y. Gershtein, F. Petriello, S. Quackenbush and K. M. Zurek, Phys. Rev. D **78**, 095002 (2008) [arXiv:0809.2849 [hep-ph]].

[5] F. J. Petriello, S. Quackenbush and K. M. Zurek, Phys. Rev. D **77**, 115020 (2008) [arXiv:0803.4005 [hep-ph]].

[6] L. M. Carpenter, A. Nelson, C. Shimmin, T. M. P. Tait and D. Whiteson, Phys. Rev. D **87**, no. 7, 074005 (2013) [arXiv:1212.3352].

[7] Y. Bai and T. M. P. Tait, Phys. Lett. B **723**, 384 (2013) [arXiv:1208.4361 [hep-ph]].

[8] A. A. Petrov and W. Shepherd, Phys. Lett. B **730**, 178 (2014) [arXiv:1311.1511 [hep-ph]].

[9] T. Lin, E. W. Kolb and L. T. Wang, Phys. Rev. D **88**, no. 6, 063510 (2013) [arXiv:1303.6638 [hep-ph]].

[10] G. Aad *et al.* [ATLAS Collaboration], JHEP **1303**, 128 (2013) [arXiv:1211.6096 [hep-ex]].

[11] J. Goodman, M. Ibe, A. Rajaraman, W. Shepherd, T. M. P. Tait and H. B. Yu, Phys. Lett. B **695**, 185 (2011) [arXiv:1005.1286 [hep-ph]].

[12] M. Beltran, D. Hooper, E. W. Kolb and Z. C. Krusberg, Phys. Rev. D **80**, 043509 (2009) [arXiv:0808.3384 [hep-ph]].

[13] W. Shepherd, T. M. P. Tait and G. Zaharijas, Phys. Rev. D **79**, 055022 (2009) [arXiv:0901.2125 [hep-ph]].

[14] Q. H. Cao, C. R. Chen, C. S. Li and H. Zhang, JHEP **1108**, 018 (2011) [arXiv:0912.4511 [hep-ph]].

[15] Y. Bai, P. J. Fox and R. Harnik, JHEP **1012**, 048 (2010) [arXiv:1005.3797 [hep-ph]].

[16] A. Rajaraman, W. Shepherd, T. M. P. Tait and A. M. Wijangco, Phys. Rev. D **84**, 095013 (2011) [arXiv:1108.1196 [hep-ph]].

[17] P. J. Fox, R. Harnik, J. Kopp and Y. Tsai, Phys. Rev. D **85**, 056011 (2012) [arXiv:1109.4398 [hep-ph]].

[18] K. Cheung, P. Y. Tseng, Y. L. S. Tsai and T. C. Yuan, JCAP **1205**, 001 (2012) [arXiv:1201.3402 [hep-ph]].

[19] A. Alves, S. Profumo and F. S. Queiroz, JHEP **1404**, 063 (2014) [arXiv:1312.5281 [hep-ph]].

[20] M. Chala, F. Kahlhoefer, M. McCullough, G. Nardini and K. Schmidt-Hoberg, JHEP **1507**, 089 (2015) [arXiv:1503.05916 [hep-ph]].

[21] A. Alloul, N. D. Christensen, C. Degrande, C. Duhr and B. Fuks, Comput. Phys. Commun. **185**, 2250 (2014) [arXiv:1310.1921 [hep-ph]].

[22] J. Alwall, M. Herquet, F. Maltoni, O. Mattelaer and T. Stelzer, J. High Energy Phys. **06**, 128 (2011) [arXiv:1106.0522 [hep-ph]].

[23] T. Sjostrand, S. Mrenna and P. Z. Skands, J. High Energy Phys. **05**, 026 (2006) [hep-ph/0603175].

[24] J. de Favereau *et al.* [DELPHES 3 Collaboration], JHEP **1402**, 057 (2014) [arXiv:1307.6346 [hep-ex]].

[25] M. L. Mangano, M. Moretti, F. Piccinini and M. Treccani, JHEP **0701**, 013 (2007) [hep-ph/0611129].

[26] P. J. Fox and C. Williams, Phys. Rev. D **87**, no. 5, 054030 (2013) [arXiv:1211.6390 [hep-ph]].

[27] U. Haisch, F. Kahlhoefer and E. Re, JHEP **1312**, 007 (2013) [arXiv:1310.4491 [hep-ph]].

[28] L. Edelhuser, M. Krmer and J. Sonneveld, JHEP **1504**, 146 (2015) [arXiv:1501.03942 [hep-ph]].

[29] A. J. Barr, JHEP **0602**, 042 (2006) [hep-ph/0511115].

[30] A. Alves and O. Eboli, Phys. Rev. D **75**, 115013 (2007) [arXiv:0704.0254 [hep-ph]].

[31] D. R. Tovey, JHEP **0804**, 034 (2008) [arXiv:0802.2879 [hep-ph]].

[32] T. Melia, JHEP **1201**, 143 (2012) [arXiv:1110.6185 [hep-ph]].

[33] T. Aaltonen *et al.* [CDF Collaboration], Phys. Rev. D **82**, 112005 (2010) [arXiv:1004.1181 [hep-ex]].

[34] R. D. Cousins, J. T. Linneman and J. Tucker, Nuclear Instruments and Methods in Physics Research A 595 (2008) 480–501 [arXiv:physics/0702156].

[35] Ti-Pei Li and Yu-qian Ma, Astrophysical Journal **272**, 317 (1983).

[36] V. Khachatryan *et al.* [CMS Collaboration], arXiv:1503.05467 [hep-ex].

[37] V. M. Abazov *et al.* [D0 Collaboration], Phys. Rev. D **78**, 012005 (2008) [arXiv:0803.0739 [hep-ex]].

[38] R. J. Barlow, J. Comput. Phys. **72**, 202 (1987).

[39] For a similar application of $\mathcal{D}_{LF}$ techniques in DM hunting, M. A. Gomez, C. B. Jackson and G. Shaughnessy, JCAP **1412**, no. 12, 025 (2014) [arXiv:1404.1918 [hep-ph]].

[40] H. B. Prosper, PoS ACAT **08**, 010 (2008).

[41] ROOT, An Object-Oriented Data Analysis Framework, http://root.cern.ch.